# Intermittency of Arctic-midlatitude teleconnections: stratospheric pathway between autumn sea ice and the winter NAO

Peter Yu Feng Siew[1,2], Camille Li[1,2], Stefan Pieter Sobolowski[3,2], and Martin Peter King[3,2]

[1]Geophysical Institute, University of Bergen, Bergen, Norway
[2]Bjerknes Centre for Climate Research, Bergen, Norway
[3]NORCE, Bergen, Norway

**Correspondence:** Peter Yu Feng Siew (yu.siew@uib.no)

**Abstract.** There is an observed relationship linking Arctic sea ice conditions in autumn to midlatitude weather the following winter. Of interest in this study is a hypothesized stratospheric pathway whereby reduced sea ice in the Barents-Kara Seas enhances upward wave activity and wave-breaking in the stratosphere, leading to a weakening of the polar vortex and a transition of the North Atlantic Oscillation (NAO) to its negative phase. A Causal Effect Networks (CEN) framework is used to explore the stratospheric pathway between late autumn Barents-Kara sea ice and the February NAO, focusing on its seasonal evolution, timescale-dependence, and robustness. Results indicate that the pathway is statistically detectable and has been relatively "active" over the 39-year observational period used here, explaining approximately 26% of the interannual variability in the February NAO. However, a bootstrap-based resampling test reveals that the pathway is highly intermittent: the full stratospheric pathway appears in only 15% of the sample populations derived from observations, with individual causal linkages ranging from 44 to 85% in occurrence rates. The pathway's intermittency is consistent with the weak signal-to-noise ratio of the atmospheric response to Arctic sea ice variability in modelling experiments, and suggests that Arctic-midlatitude teleconnections might be favoured in certain background states. On shorter time scales, the CEN detects two-way interactions between Barents-Kara sea ice and the midlatitude circulation that indicate a role for synoptic variability associated with blocking over the Urals region and moist air intrusions from the Euro-Atlantic sector. This synoptic variability has the potential to interfere with the stratospheric pathway, thereby contributing to its intermittency. This study helps quantify the robustness of causal linkages within the stratospheric pathway, and provides insight into which linkages are most subject to sampling issues within the relatively short observational record. Overall, the results should help guide the analysis and design of ensemble modelling experiments required to improve physical understanding of Arctic-midlatitude teleconnections.

## 1 Introduction

Autumn sea ice is a potential source of skill in predicting the winter North Atlantic Oscillation (NAO), and hence, European climate (Scaife et al., 2014; Wang et al., 2017; Hall et al., 2017). One proposed mechanism for the relationship focuses

on the Barents-Kara Seas, a region with seasonal ice cover that has exhibited strong negative trends during the cold season over the last decades (Cavalieri and Parkinson, 2012; Serreze and Stroeve, 2015; Onarheim and Årthun, 2017). According to

25 this mechanism, reduced Barents-Kara sea ice triggers a wave response that constructively interferes with the climatological stationary wave pattern (Peings and Magnusdottir, 2014; Kim et al., 2014; Sun et al., 2015; Nakamura et al., 2016; Wu and Smith, 2016; Hoshi et al., 2017; Zhang et al., 2018a; De and Wu, 2018), enhancing upward propagation of planetary waves that weakens the stratospheric polar vortex (Nishii et al., 2009; Garfinkel et al., 2010; Smith et al., 2010). Downward coupling from the stratosphere to the troposphere subsequently produces circulation anomalies that resemble the negative phase of the

30 NAO (Baldwin and Dunkerton, 1999; Polvani and Waugh, 2004), along with its attendant climate effects (Hurrell, 1995).

A delayed stratospheric pathway linking sea ice and the NAO is suggested by observations, but its exact nature is somewhat unclear. The observational evidence (e.g., García-Serrano et al., 2015; King et al., 2016; Koenigk et al., 2016; Kretschmer et al., 2016) hinges on lagged correlations such as the one shown in Fig. 1a (similar to Fig. 10c in García-Serrano et al. (2015) and Fig. 6b in King et al. (2016)): less Barents-Kara sea ice in November is associated with higher polar cap heights in the

35 stratosphere (i.e., polar vortex weakening), and a subsequent downward propagation of the height anomalies into the tropo-sphere through the winter season, consistent with the appearance of negative NAO conditions several months later. However, the stationarity and statistical significance of this signal has been questioned when using longer records that extend back before the satellite era (Hopsch et al., 2012; Kolstad and Screen, 2019). In fact, the signal even changes when the observational period in Fig. 1a is extended by several additional winters, showing a weaker and statistically insignificant autumn sea ice connection

40 to the winter NAO via the stratosphere (Fig. 1b).

Evidence from modelling experiments is even more difficult to interpret because the relationship between Barents-Kara sea ice and the NAO is not robust in simulations. Some studies find a clear stratospheric signal after removing sea ice, leading to a weakening of the polar vortex and a negative NAO (Kim et al., 2014; Nakamura et al., 2015; Sun et al., 2015). A negative NAO response to sea ice loss is also possible, although much weaker, if the stratospheric pathway is not well represented or artificially

45 suppressed (Liptak and Strong, 2014; Sun et al., 2015; Wu and Smith, 2016; Nakamura et al., 2016; Zhang et al., 2018a; De and Wu, 2018). However, other modelling studies show a weak or even positive NAO response when sea ice is reduced (Singarayer et al., 2006; Strey et al., 2010; Orsolini et al., 2012; Cassano et al., 2014; Screen et al., 2014). Complicating matters further, we lack a comprehensive understanding of why model results are so different (Screen et al., 2018). Possible reasons include sensitivity to where and when sea ice is removed (Sun et al., 2015; Screen, 2017; McKenna et al., 2018), nonlinearities with

50 respect to the amplitude of sea ice loss (Petoukhov and Semenov, 2010; Semenov and Latif, 2015; Chen et al., 2016; Overland et al., 2016), and dependence of the atmospheric response on the background state (Smith et al., 2017, 2019; Labe et al., 2019).

Overall, isolating the sea ice influence on the midlatitudes remains a challenge in part because it is a search for causal drivers in a tightly coupled system with large internal variability (Shepherd, 2016). This internal atmospheric varibility itself has well-known effects on Arctic climate over a range of time scales. Synoptic weather systems carry heat and moisture poleward from

55 the North Atlantic, and are associated with moist intrusions that have been shown to warm the Arctic and melt sea ice (Woods et al., 2013; Park et al., 2015a, b; Gong and Luo, 2017; Kim et al., 2017; Lee et al., 2017). Feedbacks between sea ice and NAO acting on intraseasonal time scales can yield oppsite-signed relationships depending on the time lag considered: anomalously

low Barents-Kara sea ice concentrations are favoured by positive NAO conditions (Fang and Wallace, 1994; Deser et al., 2000), but are also part of an ice perturbation pattern that has been found to produce negative NAO conditions (Magnusdottir et al.,

60  2004; Deser et al., 2004; Kvamstø et al., 2004; Strong et al., 2009; Deser et al., 2010; Wu and Zhang, 2010). The causality problem with respect to sea ice extends beyond the NAO to other midlatitude phenomena such as Eurasian cooling, for which one finds numerous studies arguing both for (Outten and Esau, 2012; Mori et al., 2014, 2019) and against (McCusker et al., 2016; Sorokina et al., 2016; Ogawa et al., 2018; Blackport et al., 2019) the existence of a linkage.

In the present study, we revisit the observed relationship between autumn Barents-Kara sea ice and the winter NAO with

65  the goal of quantifying the robustness of the stratospheric linkage. In other words, we ask how systematically the stratospheric linkage has appeared during the satellite period. While sampling issues are unavoidable when using a short observational record with large internal variability, our analysis attempts to account for this by exploring the idea that weak but statistically significant signals may arise from a teleconnection pathway that is only intermittently active.

We begin with a description of data and methods (section 2), including a Causal Effect Networks (CEN) approach that

70  provides a statistical framework for assessing causality (applied to climate problems by studies such as Ebert-Uphoff and Deng, 2012; Runge et al., 2014; Kretschmer et al., 2016). Results showing that the pathway is indeed detectable but exhibits a high level of intermittency are presented in section 3, and the implications for understanding present day Arctic-midlatitude teleconnections are discussed in section 4. We end with some concluding remarks in section 5.

## 2  Data and Methods

### 2.1  Reanalysis data

The Causal Effect Networks (CEN) approach requires indices (time series) of variables representing key processes in the dynamical mechanism being studied. In our study, we use sea ice area fraction, surface sensible heat flux, surface latent heat flux, sea level pressure, meridional wind, temperature, geopotential height, and downard thermal radiation at the surface. Raw daily data for the period 1979 to 2018 are from the European Center for Medium-Range Weather Forecasts (ECMWF) ERA-

80  Interim reanalysis (Dee et al., 2011). The seasonal cycle is removed at each grid point by subtracting the climatological daily mean to obtain anomalies of each variable, and the data are detrended. The trend is removed through all the days of the year (1 January, 2 January, etc.). The following indices are then calculated from the reanalysis data from September to March:

- Barents-Kara sea ice (ICE): sea ice area fraction averaged over 70°-80° N, 30°-105° E (Fig. 2a)

- Barents-Kara turbulent heat flux (THF): sum of surface sensible and latent heat flux averaged over 70°-80° N, 30°-105° E

85  (Fig. 2b), with positive defined as heat flux from the ocean to the atmosphere

- stratospheric polar vortex strength (SPV): negative of geopotential height poleward of 60° N (Fig. 2c) averaged between 10-100 hPa, as defined by Kretschmer et al. (2016), such that positive values of the index indicate a stronger polar vortex

- Urals sea level pressure (URALS): sea level pressure averaged over 45°-70° N, 40°-85° E (Fig. 2d)

- downward longwave radiation (IR): downward thermal radiation at the surface averaged over 70°-90° N (Fig. 2e)

90 
- poleward eddy heat flux (V*T*): product of V* and T* at 100 hPa averaged over 45°-75° N (Fig. 2f), where V and T denote the meridional wind velocity and air temperature respectively, and the superscript * indicates deviations from the zonal mean

- North Atlantic Oscillation index (NAO): from the Climate Prediction Center, based on Rotated Principal Component Analysis of 500 hPa geopotential height, see details at

95 https://www.cpc.ncep.noaa.gov/products/precip/CWlink/pna/nao.shtml

Finally, the daily indices are averaged up to monthly, half-monthly and pentad means for the different analyses carried out in this study.

## 2.2 Causal Effect Networks (CEN)

The CEN algorithm is a causal inference framework (Runge et al., 2014) aimed at identifying causal relationships between
100 variables of interest. It was previously used to study Arctic-midlatitude teleconnections by Kretschmer et al. (2016), who include a comprehensive description of the algorithm. Essentially, given a set of indices such as the ones described above, a CEN is constructed following three steps: 1) identify potential causal drivers of each index, 2) identify the true drivers from these potential drivers, and 3) quantify the strength of the causal relationships. We will illustrate how to identify and quantify the causal drivers of January stratospheric polar vortex strength ($SPV_{Jan}$) on monthly time scales as an example.

105 In the first step, we find all possible drivers for $SPV_{Jan}$. This is done by calculating the Pearson correlation $r$ between $SPV_{Jan}$ and all other indices (including SPV itself) in the preceding months, up to a maximum lag of 2 months (i.e., November and December for this example). Only indices with correlations that are significant at the 5% level (two tailed t-test; other significance levels up to 1% also tested) are considered as potential causal drivers of $SPV_{Jan}$. These are: $V*T*_{Dec}$, $URALS_{Dec}$, $SPV_{Dec}$ and $URALS_{Nov}$. This list is sorted in descending order according to the absolute value of the Pearson correlation
110 coefficient.

In the second step, we test for independence of the potential causal drivers of $SPV_{Jan}$ using partial correlations. We start with the potential causal driver that has the highest Pearson correlation with $SPV_{Jan}$, in this case $V*T*_{Dec}$, and recalculate all other correlations controlling for this driver. For example, the partial correlation between $URALS_{Nov}$ and $SPV_{Jan}$ with the effect of $V*T*_{Dec}$ removed, following the notation of Kretschmer et al. (2016), is:

115 $$\rho(URALS_{Nov}, SPV_{Jan} \mid V*T*_{Dec}) = -0.274, \tag{1}$$

where

$$\rho(x, y \mid z) = \frac{r_{xy} - r_{xz}r_{yz}}{\sqrt{1 - r_{xz}^2}\sqrt{1 - r_{yz}^2}} \tag{2}$$

The partial correlation is not significant at the 5% level (p-value = 0.105), therefore, $URALS_{Nov}$ is rejected as a causal driver of $SPV_{Jan}$. Similar partial correlation tests are carried out for $URALS_{Dec}$ (significant) and $SPV_{Dec}$ (insignificant) controlling

120 for V*T*$_{\text{Dec}}$. Thus, after controlling for V*T*$_{\text{Dec}}$, the list of potential causal drivers of SPV$_{\text{Jan}}$ is narrowed to V*T*$_{\text{Dec}}$ and URALS$_{\text{Dec}}$. We then move on to control for the variable with the next highest Pearson correlation with SPV$_{\text{Jan}}$ (URALS$_{\text{Dec}}$), and test the partial correlations for all remaining potential drivers (V*T*$_{\text{Dec}}$):

$$\rho(\text{V*T*}_{\text{Dec}}, \text{SPV}_{\text{Jan}} \mid \text{URALS}_{\text{Dec}}) = -0.512, \tag{3}$$

The partial correlation between SPV$_{\text{Jan}}$ and V*T*$_{\text{Dec}}$ is significant (p-value = 0.00142) controlling for URALS$_{\text{Dec}}$. Now all
125 combinations have been tested so the algorithm stops. (If there are more than two causal drivers left after controlling for all variables individually, the partial correlation test is repeated controlling for two drivers together, in all combinations.) The result of the second step is the identification of two causal drivers of SPV$_{\text{Jan}}$: V*T*$_{\text{Dec}}$ and URALS$_{\text{Dec}}$.

In the third step, we use a multiple regression equation to quantify the influence of causal drivers and simultaneous influences on SPV$_{\text{Jan}}$:

130 $$\text{SPV}_{\text{Jan}}^{s} = \beta_0 + \beta_1 * \text{V*T*}_{\text{Dec}}^{s} + \beta_2 * \text{URALS}_{\text{Dec}}^{s} + \beta_3 * \text{X}_{\text{Jan}}^{s} \tag{4}$$

where the $\beta$ values are regression coefficients for the standardized regressors V*T*$_{\text{Dec}}^{s}$, URALS$_{\text{Dec}}^{s}$ and X$_{\text{Jan}}^{s}$. X tests for significant simultaneous relationships between all indices and SPV$_{\text{Jan}}$, and the superscript $s$ indicates a standardized index. By standardizing, the interpretation is that changing a certain regressor by one standard deviation changes SPV$_{\text{Jan}}$ by $\beta$ standard deviations, provided that all other variables are held fixed. Note that Kretschmer et al. (2016) also included all other indices
135 (including the rejected drivers from the second step) in the multiple regression equation (Eq. (4)) along with the retained drivers. We do not adopt this approach because it somewhat arbitrarily disregards the results from the partial correlation tests in the second step. Furthermore, for this study, including the rejected drivers in the third step does not change the main results (Fig. S4 shows detected causal drivers from this additional step).

The above example illustrates how the CEN algorithm identifies and evaluates causal drivers of SPV$_{\text{Jan}}$. In order to construct
140 the complete monthly and half-monthly CENs for the stratospheric pathway, we identify causal drivers for all our chosen indices (ICE, THF, URALS, V*T*, SPV and NAO) during the extended winter season (NDJFM). September to December (January to March) indices are extracted from years 1979 to 2017 (1980 to 2018). All Pearson correlations (first step), partial correlations (second step) and the multiple regressions (third step) are thus based on indices with a sample size of 39 winter seasons. A similar procedure is used for the pentad CEN, but with a maximum lag of two pentads to capture processes occurring
145 on synoptic time scales.

Readers are refered to Runge et al. (2014) and Kretschmer et al. (2016) for additional details regarding the CEN algorithm.

## 3 Results

This section describes results from our exploration of the ICE-NAO stratospheric pathway using the CEN framework (section 3.1), including an assessment of its intermittency (section 3.2) and strength (section 3.3) in the observational record.
150 We also explore processes occurring on shorter timescales, and discuss how these effects may reinforce or interfere with the stratospheric pathway (section 3.4).

### 3.1 Seasonally evolving ICE-NAO pathway

We begin by examining pathways from Barents-Kara sea ice to the NAO proposed by previous studies. The CEN analysis follows the approach of Kretschmer et al. (2016), but keeps individual months separate rather than considering the DJF period as a whole. This allows us to capture the seasonal evolution of a pathway through the cold season.

The CEN (Fig. 3) shows evidence for a stratospheric pathway leading from autumn sea ice perturbations in the Barents-Kara Seas to a late winter NAO response. This pathway appears using both monthly (Fig. 3a) and half-monthly (Fig. 3b) averages as input to the CEN, albeit with slight differences in timing. The half-monthly CEN in Fig. 3b is displayed such that half-monthly linkages (shown in Fig. S2) are aggregated into full months to allow for direct comparison to Fig. 3a. Using the finer half-monthly resolution in the CEN prevents shorter timescales processes (such as linkages through THF) from being averaged out.

Coloured arrows in the network diagrams highlight the ICE-NAO stratospheric pathway, where red indicates positive relationships and blue indicates negative relationships. Grey arrows show other linkages that are statistically significant, including some tropospheric pathways that also contribute to the ICE-NAO relationship. A figure including all the identified causal linkages and autocorrelations appears in the supplementary material (Fig. S1). For the monthly CEN, the stratospheric pathway is:

$$\downarrow \text{ICE}_{\text{Oct}} \Rightarrow \uparrow \text{URALS}_{\text{Dec}} \Rightarrow \uparrow \text{V*T*}_{\text{Dec}} \Rightarrow \downarrow \text{SPV}_{\text{Jan}} \Rightarrow \downarrow \text{NAO}_{\text{Feb}}$$

For the half-monthly CEN, the pathway may be summarized as:

$$\downarrow \text{ICE}_{\text{Oct/Nov}} \Rightarrow \uparrow \text{THF}_{\text{Nov}} \Rightarrow \uparrow \text{URALS}_{\text{Dec}} \Rightarrow \uparrow \text{V*T*}_{\text{Dec/Jan}} \Rightarrow \downarrow \text{SPV}_{\text{Jan}} \Rightarrow \downarrow \text{NAO}_{\text{Feb}}$$

where we use the notation A $\Rightarrow$ B to indicate index A as a "driver" of index B, and $\downarrow$ and $\uparrow$ to represent a decrease or increase, respectively, of the indices. The pathway is described for the case of a negative sea ice perturbation leading to a negative NAO. We will focus on the monthly CEN; results from the half-monthly CEN yield consistent messages, and will be brought into the discussion where relevant.

The CEN results illustrate how the stratospheric pathway unfolds through the winter season. The timing is in general agreement with previous observational studies, suggesting that the involvement of the stratosphere introduces a few months' delay in the NAO response to Barents-Kara sea ice variability (Kim et al., 2014; García-Serrano et al., 2015; Jaiser et al., 2016; King et al., 2016; Kretschmer et al., 2016; Yang et al., 2016). The causal linkages are consistent with the idea that Arctic sea ice reduction enhances upward wave activity through constructive interference between forced Rossby waves and the climatological stationary waves (Garfinkel et al., 2010; Smith et al., 2010). The resulting increase in wave-breaking in the stratosphere decelerates the polar vortex (Charney and Drazin, 1961), which in turn leads to tropospheric circulation anomalies and surface impacts via downward coupling (Baldwin and Dunkerton, 1999). Some features of the pathway, such as the relatively long lagged relationship of autumn sea ice to December Urals sea level pressure, are not well understood, an issue that will be further discussed in section 4.

### 3.2 Intermittency of the pathway

185 The ICE-NAO stratospheric pathway identified by the CEN comprises statistical relationships inferred from a relatively short observational record of only 39 winters. It is meaningful to ask how robust the pathway is, that is, how systematically the relevant statistical relationships occur in the record. To assess the robustness, we perform a bootstrapping test, where bootstrap samples are created by randomly selecting 39 winters with replacement from the entire 1979/80-2017/18 period. The CEN of each sample is then constructed. This procedure is repeated 10000 times.

190 The bootstrapping results (Fig. 4) indicate that the stratospheric pathway is intermittent. Percentages in Fig. 4 show the occurrence rate of individual segments in the pathway within the bootstrapped sample population (see Fig. S5 for occurrence rates of other statistically significant linkages). By this measure, it is clear that individual segments have varying levels of intermittency. For example, the causal linkage $\uparrow$ V*T*$_{\mathrm{Dec}}$ $\Rightarrow$ $\downarrow$ SPV$_{\mathrm{Jan}}$ is identified in 85% of the samples, while the downward coupling linkage ($\downarrow$ SPV$_{\mathrm{Jan}}$ $\Rightarrow$ $\downarrow$ NAO$_{\mathrm{Feb}}$) is identified in only 49% of the samples. The full stratospheric pathway (the sequence 195 of all four segments) is detected in only 15% of the samples, suggesting that it does not occur systematically during every winter season. These results are consistent with previous findings suggesting that internal variability strongly modulates the influence of Arctic sea ice on the midlatitude circulation (Screen et al., 2014; Overland et al., 2016; Shepherd, 2016). The intermittency could also explain why the pathway itself is sensitive to the choice of observational period (Fig. 1), and suggests that it may be favoured in certain background states (Overland et al., 2016; Smith et al., 2017).

200 The strength of the segments in the pathway also exhibits large variability among the bootstrap samples. This can be seen in histograms of the beta coefficients for all segments in the pathway (Fig. 4). While the beta coefficients exhibit ranges of up to 0.5 for any given segment, the sign is always the same, indicating that the sign of the relationship between variables is robust. The observed beta coefficients (black lines) for the reanalysis period itself fall within the spread of the distributions. Note that the distributions are composed only of samples that detect that linkage, which is why they appear skewed. This is particularly 205 true for the linkages that are least robust (the first and last segments, for which the observed beta coefficients are towards the weaker end of the distributions) since the linkages are not detected in a large number of bootstrap samples, and hence, do not appear in the distributions. Overall, these results indicate that even when the stratospheric pathway is active, there is substantial interannual variability in how it manifests.

### 3.3 Strength of the pathway

210 Despite the intermittency of the stratospheric pathway, it is nevertheless interesting to explore its explanatory power for the late winter NAO during the current observational period. We employ a multiple linear regression framework to do this. The amount of February NAO variance explained is evaluated by considering the contribution from each step within the pathway. The full pathway can be represented by the following regression equation:

$$\mathrm{NAO}_{\mathrm{Feb}} = \beta_0 + \beta_1 \cdot \mathrm{ICE}_{\mathrm{Oct}} + \beta_2 \cdot \mathrm{URALS}_{\mathrm{Dec}} + \beta_3 \cdot \mathrm{V*T*}_{\mathrm{Dec}} + \beta_4 \cdot \mathrm{SPV}_{\mathrm{Jan}} \qquad (5)$$

215 where $\beta_0$ is a constant and $\beta_1$, $\beta_2$, $\beta_3$, $\beta_4$ are the regression coefficients for the standardized regressors ICE$_{\mathrm{Oct}}$, URALS$_{\mathrm{Dec}}$, V*T*$_{\mathrm{Dec}}$ and SPV$_{\mathrm{Jan}}$, respectively. We quantify the importance of these regressors in three ways:

a) cumulative $NAO_{Feb}$ variance explained as regressors are included, calculated by successively adding terms in the regression equation from left to right (orange bars in Fig. 5), e.g. for $V*T*_{Dec}$:

$$NAO_{Feb} = \beta_0^a + \beta_1^a \cdot ICE_{Oct} + \beta_2^a \cdot URALS_{Dec} + \beta_3^a \cdot V*T*_{Dec} \tag{6}$$

220    b) $NAO_{Feb}$ variance explained by individual regressors, calculated via a simple bivariate regression between each regressor and $NAO_{Feb}$ (blue bars), e.g., for $V*T*_{Dec}$:

$$NAO_{Feb} = \beta_0^b + \beta_1^b \cdot V*T*_{Dec} \tag{7}$$

c) reduction in $NAO_{Feb}$ variance explained when individual regressors are removed, calculated by removing the term from the regression equation (green bars), e.g., for $V*T*_{Dec}$:

225    $$NAO_{Feb} = \beta_0^c + \beta_1^c \cdot ICE_{Oct} + \beta_2^c \cdot URALS_{Dec} + \beta_4^c \cdot SPV_{Jan} \tag{8}$$

Both the blue and green bars in Fig. 5 provide a measure of the contribution of individual regressors, while comparison of these with the orange bars gives some indication of whether information from a given regressor is redundant.

The stratospheric pathway explains 26% of the variance in the February NAO (Fig. 5). The cumulative variance explained (orange bars) increases from 11% to 26% as regressors are added (moving from left to right), indicating that each linkage in
230    the pathway adds useful information. This result is consistent with other estimates from observations, but likely represents an upper limit as the Barents-Kara sea ice and NAO relationship is shown to be particularly strong during the current reanalysis period compared to the rest of the twentieth century (Kolstad and Screen, 2019).

While successive linkages in the pathway add explanatory power, they are not independent. Comparing the orange and blue bars, we see that the increase of cumulative explained variance moving from left to right is much less than the explained
235    variance from each individual regressor. For example, while $SPV_{Jan}$ explains the most NAO variance of any individual regressor (18%), its removal from the full regression does not have much effect (3% reduction in explained variance), However, we know that variability in upward wave activity and variability in the polar vortex are closely related, so in a sense, it is not physically meaningful to consider one in isolation of the other. Removing both $V*T*_{Dec}$ and $SPV_{Jan}$ from the regression equation results in a 8% reduction (not shown) in explained variance, which is perhaps a more representative estimate of the stratosphere's
240    contribution. Sea ice appears to impart information that cannot be explained by the other three regressors (6% reduction in explained NAO variance when removed), but this may also be a result of atmosphere-ice feedbacks explored in section 3.4.

### 3.4 Synoptic linkages and interactions across times scales

In the monthly CEN analysis, there are simultaneous relationships between Barents-Kara sea ice, Urals sea level pressure and the NAO (Fig. 6) that point to linkages through shorter timescale synoptic processes. For example, the NAO shows significant
245    negative simultaneous relationships with Barents-Kara sea ice (positive NAO with reduced ice) in December, January and March, reflecting a well-known pattern of atmospheric forcing on sea ice via anomalies in surface heat fluxes driven by wind

and temperature variability (Fang and Wallace, 1994; Deser et al., 2000). Additional simultaneous relationships between sea ice, turbulent heat flux, and Urals sea level pressure are consistent with synoptic features called moist intrusions (Woods et al., 2013; Park et al., 2015b). These appear to occur preferentially during the positive phase of the NAO (Luo et al., 2017) and have

250    been shown to enhance downward longwave radiation and cause sea ice reduction (Gong and Luo, 2017; Chen et al., 2018). We explore the possible influence of this moist intrusion pathway within the CEN framework by using higher frequency data to capture the relevant synoptic processes. The input data are pentad (5-day) means of Barents-Kara sea ice (ICE), Urals sea level pressure (URALS) and downward longwave radiation (IR). The maximum lag is set to two pentads (10 days) to isolate the synoptic timescale. Autocorrelation is strong on these short time scales, and thus is not used to reject causal linkages in the

255    partial correlation test.

The CEN detects synoptic-scale influences from the Arctic to the midlatitudes that reinforce linkages found in the monthly analysis. The results are summarized in Fig. 7 by summing the number of times each linkage appears over the extended winter season (i.e., the number of arrows between each pair of indices in Fig. S6). The maximum possible count for NDJFM is 60 between each pair (i.e., 5 months, 6 pentads in a month, and 2-pentad lag). Some linkages are farily systematic, for example,

260    the relationship between reduced Barents-Kara sea ice and enhanced downward longwave radiation ($\downarrow$ ICE $\Rightarrow$ $\uparrow$ IR detected in 15 out of the 60 winter pentads). This linkage is consistent with the idea that sea ice retreat exposes open ocean, which is a local evaporative source for water vapour (Kim and Kim, 2017; Zhong et al., 2018). A linkage from $\uparrow$ IR $\Rightarrow$ $\uparrow$ URALS (detected in 11/60 pentads) then points to a possible mechanism whereby the resulting surface warming weakens zonal wind locally and promotes blocking over the Urals (Luo et al., 2016). Overall, these Arctic-to-midlatitude processes should reinforce

265    the stratospheric pathway (Fig. 3), despite some interference effects (e.g., a few pentads in the ICE $\Rightarrow$ IR and ICE $\Rightarrow$ URALS counts, coloured red, where the linkage is in the opposite sign of the expected signal).

At the same time, causal effects from the midlatitudes to the Arctic are also detected, consistent with an influence from moist intrusions. This shows up in the form of linkages between $\downarrow$ URALS $\Rightarrow$ $\uparrow$ IR (detected in 9/60 pentads) and between $\uparrow$ IR $\Rightarrow$ $\downarrow$ ICE (the most robust in this analysis, detected in 21/60 pentads), as would be expected from the transport of moist

270    air into the dry Arctic atmosphere. We also detect a direct linkage to Barents-Kara sea ice ($\uparrow$ URALS $\Rightarrow$ $\downarrow$ ICE), that can be interpreted as a direct effect of warm air advection and mechanical forcing from enhanced southerlies over the Barents-Kara region (Sorokina et al., 2016; McCusker et al., 2016).

Results in this section show two-way synoptic interactions between sea ice and the midlatitudes that indicate the presence of strong feedbacks in the system (see also King et al., 2016). Across the synoptic to seasonal timescales, it appears that sea

275    ice is best thought of as an intermediary rather than a true boundary forcing, as is implied by prescribed sea ice (e.g., AGCM) experiments. Given that our understanding of Arctic-midlatitude teleconnections must account for the combined influences of such linkages across regions and time scales, it is no surprise that we have yet to agree on a definitive set of mechanisms.

## 4 Discussion

This study quantifies the robustness of atmospheric teleconnections between the Arctic and midlatitudes, documenting their
high level of intermittency in the observational record. In a bootstrapping test, the full stratospheric pathway emerges in only
15% of the sample populations derived from the observations (Fig. 4). The existence of intermittency is likely why studies
using various analytical approaches and time periods find teleconnections that differ in pattern, timing, robustness and apparent
mechanisms (Overland et al., 2016; Francis, 2017; Cohen et al., 2018; Overland and Wang, 2018). In this section we discuss
some of the possible factors that contribute to the intermittency.

To be more concrete, the intermittency of the stratospheric pathway stems from the fact that it can be reinforced or interrupted
by other processes. For example, reinforcement can come from tropospheric pathways also detected by the CEN algorithm (see
Fig. S1a and S1b):

1) $\downarrow \text{ICE}_{\text{Oct}} \Rightarrow \uparrow \text{THF}_{\text{Nov}} \Rightarrow \uparrow \text{URALS}_{\text{Jan}} \Rightarrow \uparrow \text{URALS}_{\text{Feb}} \Rightarrow \downarrow \text{NAO}_{\text{Mar}}$

2) $\downarrow \text{ICE}_{\text{Jan}} \Rightarrow \uparrow \text{URALS}_{\text{Feb}} \Rightarrow \downarrow \text{NAO}_{\text{Mar}}$

3) $\downarrow \text{ICE}_{\text{Nov}} \Rightarrow \downarrow \text{NAO}_{\text{Jan}}$

4) $\downarrow \text{ICE}_{\text{Jan}} \Rightarrow \downarrow \text{NAO}_{\text{Mar}}$

All these tropospheric and stratospheric pathways lead from the reduction of sea ice to a negative NAO, although they differ
slightly in timing. The existence of the tropospheric pathway is supported by sea ice and surface heating perturbation experi-
ments, where negative NAO/AO responses are simulated even when the stratospheric pathway is suppressed (Wu and Smith,
2016) or not well represented (Sun et al., 2015). However, the NAO/AO response is stronger when the stratospheric pathway
is active than through the tropospheric pathway alone (Nakamura et al., 2016; Zhang et al., 2018a, b). Another example of a
factor that may contribute to intermittency is the El Niño Southern Oscillation (ENSO). El Niño winters are associated with
a deepened Aleutian low, which enhances upward propagating waves, weakens the polar vortex, and favours negative NAO
conditions (Domeisen et al., 2019). As such, the stratospheric pathway may be reinforced if an El Niño develops following a
low autumn ice season (both are associated with a weakened polar vortex, e.g., winter 1986/87 or 2009/10, see Fig. S7); if a
La Niña develops instead, the stratospheric pathway may be weakened (e.g., winter 2007/08 or 2010/11, see Fig. S7). In fact,
variability in the strength of the polar vortex for whatever reason (including internal variability) can be seen as a source of
intermittency for the pathway.

In terms of reinforcing the stratospheric pathway, blocking over the Urals region seems to play a particularly important,
but not fully understood, role. Enhanced Urals sea level pressure appears as a linkage in both the monthly ($\downarrow \text{ICE}_{\text{Oct}} \Rightarrow \uparrow$
$\text{URALS}_{\text{Dec}} \Rightarrow \uparrow \text{V*T*}_{\text{Dec}}$ in Fig. 3a) and half-monthly ($\downarrow \text{ICE}_{\text{Nov}} \Rightarrow \uparrow \text{URALS}_{\text{Dec}} \Rightarrow \uparrow \text{V*T*}_{\text{Jan}}$ in Fig. 3b) CEN. The latter
segment from Urals sea level pressure to poleward eddy heat flux is fairly systematic (appears in 74% of the bootstrap samples
in Fig. 4) and grounded in the idea that tropospheric precursors over the Urals lead polar vortex weakening (Cohen and Jones,
2011; Cohen et al., 2014a). However, the first segment from Barents-Kara sea ice to Urals blocking is more intermittent

310 (appears in 44% of the bootstrap samples), and whether it is in fact a causal linkage has been questioned by a recent modelling study using ensemble nudging experiments (Peings, 2019).

The ICE-URALS relationship highlights the complexity of interactions between atmospheric internal variability and Barents-Kara sea ice over a range of time scales. On synoptic scales, the pentad CEN (Fig. 7) shows linkages from reduced sea ice to enhanced Urals sea level pressure, but also linkages in the opposite direction ($\uparrow$ URALS $\Rightarrow \uparrow$ IR $\Rightarrow \downarrow$ ICE), with Urals sea

315 level pressure altering ice cover via changes in poleward moisture transport that have been tied to synoptic moist intrusions (Woods et al., 2013; Luo et al., 2016; Gong and Luo, 2017; Lee et al., 2017). This process can act as a positive feedback on sea ice perturbations, but also provides a pathway by which blocking variability (internal to the atmosphere) may interrupt the expected stratosphere-troposphere coupling signal from autumn sea ice. Furthermore, enhanced Urals blocking and moist intrusions can lead to highly transient perturbations in turbulent heat flux over Barents-Kara Seas. Initially, turbulent heat loss

320 from the ocean is suppressed near the sea ice edge where moist intrusions act to weaken temperature and moisture contrasts between the atmosphere and ocean (Woods et al., 2013; Gong and Luo, 2017), but the heat flux anomaly can become positive (enhanced heat loss from the ocean) after the sea ice melts back in response to the moist intrusion, one to two weeks later (Woods and Caballero, 2016; Lee et al., 2017). On even longer (monthly to seasonal) time scales, there is evidence that atmospheric variability is the main driver of heat flux variability over the Barents-Kara Seas both in observations and models

325 (Sorokina et al., 2016; Blackport et al., 2019), perhaps explaining why turbulent heat flux does not show up in the monthly CEN (Fig. 3a), but does in the half-monthly CEN (Fig. 3b).

A further impediment to clarifying the $\downarrow$ ICE$_{Oct} \Rightarrow \uparrow$ URALS$_{Dec}$ relationship is that the proposed mechanisms underlying the linkage act on time scales that are inconsistent with the 2-month delay found in observations. For example, reduced sea ice may allow more heating of the atmosphere by the ocean to produce a Rossby wave train with an anomalous high over the Urals

330 region (Honda et al., 2009), but this would be expected to set up within a matter of days to a week. Alternatively, reduced ice may reduce local baroclinicity, which discourages cyclones from tracking into the Barents-Kara Seas and produces an anomalous high due to the relative absence of low-pressure systems (Inoue et al., 2012). This mechanism could introduce some delay between the ice perturbation and sea level pressure perturbation, but two months still seems rather long. Finally, reduced ice may increase atmospheric moisture content, leading to increased Eurasian snow cover, diabatic cooling and anomalously

335 high sea level pressure over the continent (Liu et al., 2012; Cohen et al., 2014a; Garcia-Serrano and Frankignoul, 2014). As recent observational and modelling studies do not support a role for Eurasian snow in this teleconnection (Kretschmer et al., 2016; Peings et al., 2017; Henderson et al., 2018), we chose not to include it in our main analyses. Note that these mechanisms may still be responsible for contemporaneous forcing of the winter atmospheric circulation by winter sea ice variability, which has been suggested to be a stronger influence than the forcing by autumn sea ice variability (Blackport and Screen, 2019).

340 Lastly, our experience with the CEN offers some cautionary notes about its application to climate problems. The CEN approach was designed for hypothesis testing - that is, to test causal pathways that are thought or known to exist, either from theory or existing evidence. It should not be used as an exploratory data analysis tool to search for causal pathways a posteriori, because the statistics behind the CEN do not know whether relationships are physically meaningful. One specific problem we encountered is that the algorithm may drop an existing causal linkage if a new variable is added because the partial correlations

345 in step two change (see section 2.2). For example, when we introduce downward longwave radiation into the monthly CEN, its strong correlation with sea ice overrides the $\downarrow ICE_{Jan} \Rightarrow \uparrow URALS_{Feb}$ linkage (see Fig. S8 compared to Fig. S1a). Since many climate variables are highly correlated, the CEN's ability to identify physically meaningful linkages depends critically on the selection of input variables associated with physically meaningful mechanisms.

## 5 Concluding remarks

350 This study uses the Causal Effect Networks (CEN) framework to quantify the robustness of the stratospheric pathway between late autumn Barents-Kara sea ice and the February NAO, documenting its high level of intermittency in the observational record. The pathway has been relatively "active" over the satellite period, explaining approximately 26% of the interannual variability in the February NAO. However, this result is highly sensitive to which winters are included in the analysis. Results from a bootstrapping test show that the full stratospheric pathway appears in only 15% of the sample populations derived

355 from the observations. The result reflects the strong internal variability of the midlatitude atmosphere and the likelihood that Arctic-midlatitude teleconnections may require certain background flow conditions. On synoptic time scales, we identify two-way interactions between Barents-Kara sea ice and the midlatitude circulation suggesting a role for atmospheric blocking over the Urals region and moist intrusions, both of which can cause reduced Barents-Kara sea ice. These synoptic processes can reinforce or interrupt the stratospheric pathway, contributing to intermittency. Finally, we can not rule out that the causal

360 linkages found on longer time scales may be artefacts of averaging over the synoptic processes, or even the result of an entirely different mechanism (Smith et al., 2017; Hell et al.).

Coupled interactions between sea ice and the midlatitude circulation involve complicated lead-lag feedbacks over a range of time scales. Applying causal inference frameworks such as the CEN can help clarify some of the important physical processes at play, but in the end, models are required to improve our understanding. A complication is that the fidelity of climate models

365 in representing the relevant processes is difficult to ascertain (King et al., 2016; Smith et al., 2017; Mori et al., 2019), especially those processes at fine spatial and temporal scales and the interactions across scales. But ways forward are indicated by studies such as this (along with others, e.g., McCusker et al., 2016; Sun et al., 2016; Peings, 2019) by providing insight into the which linkages are most robust, and which are subject to sampling issues within the relatively short observational record.

*Code availability.* The codes to construct the CEN are available online at: https://github.com/petersiew/CEN

370 *Data availability.* ERA-Interim data are provided by European Centre for Medium-Range Weather Forecasts (ECMWF) online at :https://www.ecmwf.int/en/forecasts/datasets/reanalysis-datasets/era-interim

*Author contributions.* PS conducted the analysis, prepared the figures, and wrote the paper with contributions from all co-authors. CL and SPS conceived of the original idea. CL, SPS and MPK provided guidance on the interpretation of results.

*Competing interests.* Camille Li is a member of the editorial board of the journal.

375 *Acknowledgements.* This work was supported by the Research Council of Norway, project no. 255027 (DynAMiTe) and project no. 272721 (Nansen Legacy). We acknowledge the European Centre for Medium-Range Weather Forecasts for providing the ERA-Interim data. Finally, we thank all members of the Bjerknes storm tracks research group for stimulating discussions that helped improve this study.

## References

Baldwin, M. P. and Dunkerton, T. J.: Propagation of the Arctic Oscillation from the stratosphere to the troposphere, Journal of Geophysical
  Research: Atmospheres, 104, 30 937–30 946, 1999.

Blackport, R. and Screen, J. A.: Influence of Arctic Sea Ice Loss in Autumn Compared to That in Winter on the Atmospheric Circulation,
  Geophysical Research Letters, 46, 2213–2221, 2019.

Blackport, R., Screen, J. A., van der Wiel, K., and Bintanja, R.: Minimal influence of reduced Arctic sea ice on coincident cold winters in
  mid-latitudes, Nature Climate Change, 9, 697–704, 2019.

Cassano, E. N., Cassano, J. J., Higgins, M. E., and Serreze, M. C.: Atmospheric impacts of an Arctic sea ice minimum as seen in the
  Community Atmosphere Model, International Journal of Climatology, 34, 766–779, 2014.

Cavalieri, D. J. and Parkinson, C. L.: Arctic sea ice variability and trends, 1979-2010, The Cryosphere, 6, 881, 2012.

Charney, J. G. and Drazin, P. G.: Propagation of planetary-scale disturbances from the lower into the upper atmosphere, Journal of Geophys-
  ical Research, 66, 83–109, 1961.

Chen, H. W., Zhang, F., and Alley, R. B.: The robustness of midlatitude weather pattern changes due to Arctic sea ice loss, Journal of Climate,
  29, 7831–7849, 2016.

Chen, X., Luo, D., Feldstein, S. B., and Lee, S.: Impact of winter Ural blocking on Arctic sea ice: short-time variability, Journal of Climate,
  31, 2267–2282, 2018.

Cohen, J. and Jones, J.: Tropospheric precursors and stratospheric warmings, Journal of climate, 24, 6562–6572, 2011.

Cohen, J., Furtado, J. C., Jones, J., Barlow, M., Whittleston, D., and Entekhabi, D.: Linking Siberian snow cover to precursors of stratospheric
  variability, Journal of Climate, 27, 5422–5432, 2014a.

Cohen, J., Zhang, X., Francis, J., Jung, T., Kwok, R., Overland, J., Tayler, P., Lee, S., Laliberte, F., Feldstein, S., et al.: Arctic change and
  possible influence on mid-latitude climate and weather, US CLIVAR Report, 1, 2018.

De, B. and Wu, Y.: Robustness of the stratospheric pathway in linking the Barents-Kara Sea sea ice variability to the mid-latitude circulation
  in CMIP5 models, Climate Dynamics, pp. 1–15, 2018.

Dee, D. P., Uppala, S., Simmons, A., Berrisford, P., Poli, P., Kobayashi, S., Andrae, U., Balmaseda, M., Balsamo, G., Bauer, d. P., et al.: The
  ERA-Interim reanalysis: Configuration and performance of the data assimilation system, Quarterly Journal of the royal meteorological
  society, 137, 553–597, 2011.

Deser, C., Walsh, J. E., and Timlin, M. S.: Arctic sea ice variability in the context of recent atmospheric circulation trends, Journal of Climate,
  13, 617–633, 2000.

Deser, C., Magnusdottir, G., Saravanan, R., and Phillips, A.: The effects of North Atlantic SST and sea ice anomalies on the winter circulation
  in CCM3. Part II: Direct and indirect components of the response, Journal of Climate, 17, 877–889, 2004.

Deser, C., Tomas, R., Alexander, M., and Lawrence, D.: The seasonal atmospheric response to projected Arctic sea ice loss in the late
  twenty-first century, Journal of Climate, 23, 333–351, 2010.

Domeisen, D. I., Garfinkel, C. I., and Butler, A. H.: The teleconnection of El Niño Southern Oscillation to the stratosphere, Reviews of
  Geophysics, 57, 5–47, 2019.

Ebert-Uphoff, I. and Deng, Y.: Causal discovery for climate research using graphical models, Journal of Climate, 25, 5648–5665, 2012.

Fang, Z. and Wallace, J. M.: Arctic sea ice variability on a timescale of weeks and its relation to atmospheric forcing, Journal of Climate, 7,
  1897–1914, 1994.

415   Francis, J. A.: Why are Arctic linkages to extreme weather still up in the air?, Bulletin of the American Meteorological Society, 98, 2551–
         2557, 2017.

       Garcia-Serrano, J. and Frankignoul, C.: Retraction: High predictability of the winter Euro–Atlantic climate from cryospheric variability,
         2014.

       García-Serrano, J., Frankignoul, C., Gastineau, G., and De La Càmara, A.: On the predictability of the winter Euro-Atlantic climate: lagged
420      influence of autumn Arctic sea ice, Journal of Climate, 28, 5195–5216, 2015.

       Garfinkel, C. I., Hartmann, D. L., and Sassi, F.: Tropospheric precursors of anomalous Northern Hemisphere stratospheric polar vortices,
         Journal of Climate, 23, 3282–3299, 2010.

       Gong, T. and Luo, D.: Ural blocking as an amplifier of the Arctic sea ice decline in winter, Journal of Climate, 30, 2639–2654, 2017.

       Hall, R. J., Scaife, A. A., Hanna, E., Jones, J. M., and Erdélyi, R.: Simple statistical probabilistic forecasts of the winter NAO, Weather and
425      Forecasting, 32, 1585–1601, 2017.

       Hell, M., Schneider, T., and Li, C.: Atmospheric response to episodic Arctic warming in an idealized model, Journal of Climate.

       Henderson, G. R., Peings, Y., Furtado, J. C., and Kushner, P. J.: Snow–atmosphere coupling in the Northern Hemisphere, Nature Climate
         Change, 8, 954–963, 2018.

       Honda, M., Inoue, J., and Yamane, S.: Influence of low Arctic sea-ice minima on anomalously cold Eurasian winters, Geophysical Research
430      Letters, 36, 2009.

       Hopsch, S., Cohen, J., and Dethloff, K.: Analysis of a link between fall Arctic sea ice concentration and atmospheric patterns in the following
         winter, Tellus A: Dynamic Meteorology and Oceanography, 64, 18 624, 2012.

       Hoshi, K., Ukita, J., Honda, M., Iwamoto, K., Nakamura, T., Yamazaki, K., Dethloff, K., Jaiser, R., and Handorf, D.: Poleward eddy heat
         flux anomalies associated with recent Arctic sea ice loss, Geophysical Research Letters, 44, 446–454, 2017.

435   Hurrell, J. W.: Decadal trends in the North Atlantic Oscillation: regional temperatures and precipitation, Science, 269, 676–679, 1995.

       Inoue, J., Hori, M. E., and Takaya, K.: The role of Barents Sea ice in the wintertime cyclone track and emergence of a warm-Arctic cold-
         Siberian anomaly, Journal of Climate, 25, 2561–2568, 2012.

       Jaiser, R., Nakamura, T., Handorf, D., Dethloff, K., Ukita, J., and Yamazaki, K.: Atmospheric winter response to Arctic sea ice changes in
         reanalysis data and model simulations, Journal of Geophysical Research: Atmospheres, 121, 7564–7577, 2016.

440   Kim, B.-M., Son, S.-W., Min, S.-K., Jeong, J.-H., Kim, S.-J., Zhang, X., Shim, T., and Yoon, J.-H.: Weakening of the stratospheric polar
         vortex by Arctic sea-ice loss, Nature communications, 5, 4646, 2014.

       Kim, B.-M., Hong, J.-Y., Jun, S.-Y., Zhang, X., Kwon, H., Kim, S.-J., Kim, J.-H., Kim, S.-W., and Kim, H.-K.: Major cause of unprecedented
         Arctic warming in January 2016: Critical role of an Atlantic windstorm, Scientific reports, 7, 40 051, 2017.

       Kim, H.-M. and Kim, B.-M.: Relative contributions of atmospheric energy transport and sea ice loss to the recent warm Arctic winter, Journal
445      of Climate, 30, 7441–7450, 2017.

       King, M. P., Hell, M., and Keenlyside, N.: Investigation of the atmospheric mechanisms related to the autumn sea ice and winter circulation
         link in the Northern Hemisphere, Climate dynamics, 46, 1185–1195, 2016.

       Koenigk, T., Caian, M., Nikulin, G., and Schimanke, S.: Regional Arctic sea ice variations as predictor for winter climate conditions, Climate
         Dynamics, 46, 317–337, 2016.

450   Kolstad, E. and Screen, J.: Non-Stationary Relationship between Autumn Arctic Sea Ice and the Winter North Atlantic Oscillation, Geophys-
         ical Research Letters, 2019.

Kretschmer, M., Coumou, D., Donges, J. F., and Runge, J.: Using causal effect networks to analyze different Arctic drivers of midlatitude winter circulation, Journal of Climate, 29, 4069–4081, 2016.

Kvamstø, N. G., Skeie, P., and Stephenson, D. B.: Impact of Labrador sea-ice extent on the North Atlantic Oscillation, International Journal
455    of Climatology: A Journal of the Royal Meteorological Society, 24, 603–612, 2004.

Labe, Z., Peings, Y., and Magnusdottir, G.: The Effect of QBO Phase on the Atmospheric Response to Projected Arctic Sea Ice Loss in Early Winter, Geophysical Research Letters, 46, 7663–7671, 2019.

Lee, S., Gong, T., Feldstein, S. B., Screen, J. A., and Simmonds, I.: Revisiting the cause of the 1989–2009 Arctic surface warming using the surface energy budget: downward infrared radiation dominates the surface fluxes, Geophysical research letters, 44, 10–654, 2017.

460    Liptak, J. and Strong, C.: The winter atmospheric response to sea ice anomalies in the Barents Sea, Journal of Climate, 27, 914–924, 2014.

Liu, J., Curry, J. A., Wang, H., Song, M., and Horton, R. M.: Impact of declining Arctic sea ice on winter snowfall, Proceedings of the National Academy of Sciences, 109, 4074–4079, 2012.

Luo, B., Luo, D., Wu, L., Zhong, L., and Simmonds, I.: Atmospheric circulation patterns which promote winter Arctic sea ice decline, Environmental Research Letters, 12, 054 017, 2017.

465    Luo, D., Xiao, Y., Diao, Y., Dai, A., Franzke, C. L., and Simmonds, I.: Impact of Ural blocking on winter warm Arctic–cold Eurasian anomalies. Part II: The link to the North Atlantic Oscillation, Journal of Climate, 29, 3949–3971, 2016.

Magnusdottir, G., Deser, C., and Saravanan, R.: The effects of North Atlantic SST and sea ice anomalies on the winter circulation in CCM3. Part I: Main features and storm track characteristics of the response, Journal of Climate, 17, 857–876, 2004.

McCusker, K. E., Fyfe, J. C., and Sigmond, M.: Twenty-five winters of unexpected Eurasian cooling unlikely due to Arctic sea-ice loss,
470    Nature Geoscience, 9, 838, 2016.

McKenna, C. M., Bracegirdle, T. J., Shuckburgh, E. F., Haynes, P. H., and Joshi, M. M.: Arctic sea ice loss in different regions leads to contrasting Northern Hemisphere impacts, Geophysical Research Letters, 45, 945–954, 2018.

Mori, M., Watanabe, M., Shiogama, H., Inoue, J., and Kimoto, M.: Robust Arctic sea-ice influence on the frequent Eurasian cold winters in past decades, Nature Geoscience, 7, 869, 2014.

475    Mori, M., Kosaka, Y., Watanabe, M., Nakamura, H., and Kimoto, M.: A reconciled estimate of the influence of Arctic sea-ice loss on recent Eurasian cooling, Nature Climate Change, 9, 123, 2019.

Nakamura, T., Yamazaki, K., Iwamoto, K., Honda, M., Miyoshi, Y., Ogawa, Y., and Ukita, J.: A negative phase shift of the winter AO/NAO due to the recent Arctic sea-ice reduction in late autumn, Journal of Geophysical Research: Atmospheres, 120, 3209–3227, 2015.

Nakamura, T., Yamazaki, K., Iwamoto, K., Honda, M., Miyoshi, Y., Ogawa, Y., Tomikawa, Y., and Ukita, J.: The stratospheric pathway for
480    Arctic impacts on midlatitude climate, Geophysical Research Letters, 43, 3494–3501, 2016.

Nishii, K., Nakamura, H., and Miyasaka, T.: Modulations in the planetary wave field induced by upward-propagating Rossby wave packets prior to stratospheric sudden warming events: A case-study, Quarterly Journal of the Royal Meteorological Society: A journal of the atmospheric sciences, applied meteorology and physical oceanography, 135, 39–52, 2009.

Ogawa, F., Keenlyside, N., Gao, Y., Koenigk, T., Yang, S., Suo, L., Wang, T., Gastineau, G., Nakamura, T., Cheung, H. N., et al.: Evaluating
485    impacts of recent Arctic sea ice loss on the northern hemisphere winter climate change, Geophysical Research Letters, 45, 3255–3263, 2018.

Onarheim, I. H. and Årthun, M.: Toward an ice-free Barents Sea, Geophysical Research Letters, 44, 8387–8395, 2017.

Orsolini, Y. J., Senan, R., Benestad, R. E., and Melsom, A.: Autumn atmospheric response to the 2007 low Arctic sea ice extent in coupled ocean–atmosphere hindcasts, Climate dynamics, 38, 2437–2448, 2012.

490   Outten, S. and Esau, I.: A link between Arctic sea ice and recent cooling trends over Eurasia, Climatic Change, 110, 1069–1075, 2012.

Overland, J. E. and Wang, M.: Arctic-midlatitude weather linkages in North America, Polar Science, 16, 1–9, 2018.

Overland, J. E., Dethloff, K., Francis, J. A., Hall, R. J., Hanna, E., Kim, S.-J., Screen, J. A., Shepherd, T. G., and Vihma, T.: Nonlinear response of mid-latitude weather to the changing Arctic, Nature Climate Change, 6, 992, 2016.

Park, D.-S. R., Lee, S., and Feldstein, S. B.: Attribution of the recent winter sea ice decline over the Atlantic sector of the Arctic Ocean,
495     Journal of climate, 28, 4027–4033, 2015a.

Park, H.-S., Lee, S., Son, S.-W., Feldstein, S. B., and Kosaka, Y.: The impact of poleward moisture and sensible heat flux on Arctic winter sea ice variability, Journal of Climate, 28, 5030–5040, 2015b.

Peings, Y.: Ural Blocking as a Driver of Early-Winter Stratospheric Warmings, Geophysical Research Letters, 46, 5460–5468, 2019.

Peings, Y. and Magnusdottir, G.: Response of the wintertime Northern Hemisphere atmospheric circulation to current and projected Arctic
500     sea ice decline: A numerical study with CAM5, Journal of Climate, 27, 244–264, 2014.

Peings, Y., Douville, H., Colin, J., Martin, D. S., and Magnusdottir, G.: Snow–(N) AO teleconnection and its modulation by the Quasi-Biennial Oscillation, Journal of Climate, 30, 10 211–10 235, 2017.

Petoukhov, V. and Semenov, V. A.: A link between reduced Barents-Kara sea ice and cold winter extremes over northern continents, Journal of Geophysical Research: Atmospheres, 115, 2010.

505   Polvani, L. M. and Waugh, D. W.: Upward wave activity flux as a precursor to extreme stratospheric events and subsequent anomalous surface weather regimes, Journal of climate, 17, 3548–3554, 2004.

Runge, J., Petoukhov, V., and Kurths, J.: Quantifying the strength and delay of climatic interactions: The ambiguities of cross correlation and a novel measure based on graphical models, Journal of Climate, 27, 720–739, 2014.

Scaife, A., Arribas, A., Blockley, E., Brookshaw, A., Clark, R., Dunstone, N., Eade, R., Fereday, D., Folland, C., Gordon, M., et al.: Skillful
510     long-range prediction of European and North American winters, Geophysical Research Letters, 41, 2514–2519, 2014.

Screen, J. A.: Simulated atmospheric response to regional and pan-Arctic sea ice loss, Journal of Climate, 30, 3945–3962, 2017.

Screen, J. A., Deser, C., Simmonds, I., and Tomas, R.: Atmospheric impacts of Arctic sea-ice loss, 1979–2009: Separating forced change from atmospheric internal variability, Climate dynamics, 43, 333–344, 2014.

Screen, J. A., Deser, C., Smith, D. M., Zhang, X., Blackport, R., Kushner, P. J., Oudar, T., McCusker, K. E., and Sun, L.: Consistency and
515     discrepancy in the atmospheric response to Arctic sea-ice loss across climate models, Nature Geoscience, p. 1, 2018.

Semenov, V. A. and Latif, M.: Nonlinear winter atmospheric circulation response to Arctic sea ice concentration anomalies for different periods during 1966–2012, Environmental Research Letters, 10, 054 020, 2015.

Serreze, M. C. and Stroeve, J.: Arctic sea ice trends, variability and implications for seasonal ice forecasting, Philosophical Transactions of the Royal Society A: Mathematical, Physical and Engineering Sciences, 373, 20140 159, 2015.

520   Shepherd, T. G.: Effects of a warming Arctic, Science, 353, 989–990, 2016.

Singarayer, J. S., Bamber, J. L., and Valdes, P. J.: Twenty-first-century climate impacts from a declining Arctic sea ice cover, Journal of Climate, 19, 1109–1125, 2006.

Smith, D. M., Dunstone, N. J., Scaife, A. A., Fiedler, E. K., Copsey, D., and Hardiman, S. C.: Atmospheric response to Arctic and Antarctic sea ice: The importance of ocean–atmosphere coupling and the background state, Journal of Climate, 30, 4547–4565, 2017.

525   Smith, D. M., Screen, J. A., Deser, C., Cohen, J., Fyfe, J. C., García-Serrano, J., Jung, T., Kattsov, V., Matei, D., Msadek, R., et al.: The Polar Amplification Model Intercomparison Project (PAMIP) contribution to CMIP6: investigating the causes and consequences of polar amplification, Geoscientific Model Development, 12, 1139–1164, 2019.

Smith, K. L., Fletcher, C. G., and Kushner, P. J.: The role of linear interference in the annular mode response to extratropical surface forcing, Journal of Climate, 23, 6036–6050, 2010.

530 Sorokina, S. A., Li, C., Wettstein, J. J., and Kvamstø, N. G.: Observed atmospheric coupling between Barents Sea ice and the warm-Arctic cold-Siberian anomaly pattern, Journal of Climate, 29, 495–511, 2016.

Strey, S. T., Chapman, W. L., and Walsh, J. E.: The 2007 sea ice minimum: Impacts on the Northern Hemisphere atmosphere in late autumn and early winter, Journal of Geophysical Research: Atmospheres, 115, 2010.

Strong, C., Magnusdottir, G., and Stern, H.: Observed feedback between winter sea ice and the North Atlantic Oscillation, Journal of Climate,
535 22, 6021–6032, 2009.

Sun, L., Deser, C., and Tomas, R. A.: Mechanisms of stratospheric and tropospheric circulation response to projected Arctic sea ice loss, Journal of Climate, 28, 7824–7845, 2015.

Sun, L., Perlwitz, J., and Hoerling, M.: What caused the recent "Warm Arctic, Cold Continents" trend pattern in winter temperatures?, Geophysical Research Letters, 43, 5345–5352, 2016.

540 Wang, L., Ting, M., and Kushner, P.: A robust empirical seasonal prediction of winter NAO and surface climate, Scientific reports, 7, 279, 2017.

Woods, C. and Caballero, R.: The role of moist intrusions in winter Arctic warming and sea ice decline, Journal of Climate, 29, 4473–4485, 2016.

Woods, C., Caballero, R., and Svensson, G.: Large-scale circulation associated with moisture intrusions into the Arctic during winter, Geo-
545 physical Research Letters, 40, 4717–4721, 2013.

Wu, Q. and Zhang, X.: Observed forcing-feedback processes between Northern Hemisphere atmospheric circulation and Arctic sea ice coverage, Journal of Geophysical Research: Atmospheres, 115, 2010.

Wu, Y. and Smith, K. L.: Response of Northern Hemisphere midlatitude circulation to Arctic amplification in a simple atmospheric general circulation model, Journal of Climate, 29, 2041–2058, 2016.

550 Yang, X.-Y., Yuan, X., and Ting, M.: Dynamical link between the Barents–Kara sea ice and the Arctic Oscillation, Journal of Climate, 29, 5103–5122, 2016.

Zhang, P., Wu, Y., and Smith, K. L.: Prolonged effect of the stratospheric pathway in linking Barents-Kara Sea sea ice variability to the midlatitude circulation in a simplified model, Climate Dynamics, 50, 527–539, 2018a.

Zhang, P., Wu, Y., Simpson, I. R., Smith, K. L., Zhang, X., De, B., and Callaghan, P.: A stratospheric pathway linking a colder Siberia to
555 Barents-Kara Sea sea ice loss, Science advances, 4, eaat6025, 2018b.

Zhong, L., Hua, L., and Luo, D.: Local and external moisture sources for the Arctic warming over the Barents–Kara seas, Journal of Climate, 31, 1963–1982, 2018.
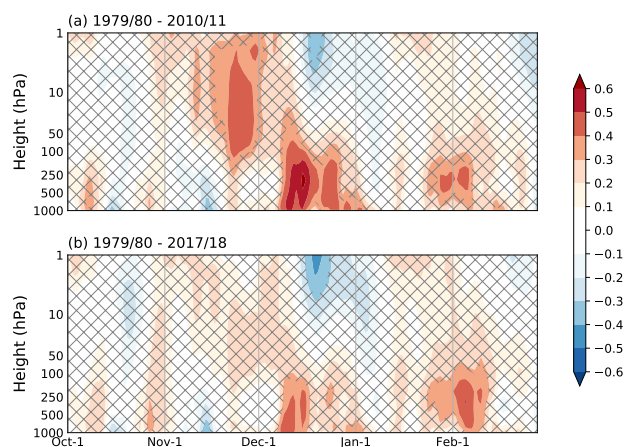
**Figure 1.** Lead-lag correlations (shading) between November Barents-Kara sea ice index (sign reversed) and polar cap height (70°N pole-ward) over the October-to-February cold season using ERA-Interim reanalysis for two periods: (a) 1979/80-2010/11 and (b) 1979/80-2017/18. Hatching indicates non-significant values at the 5% level using a two-tailed t-test. Linear trends and the seasonal cycle have been removed.
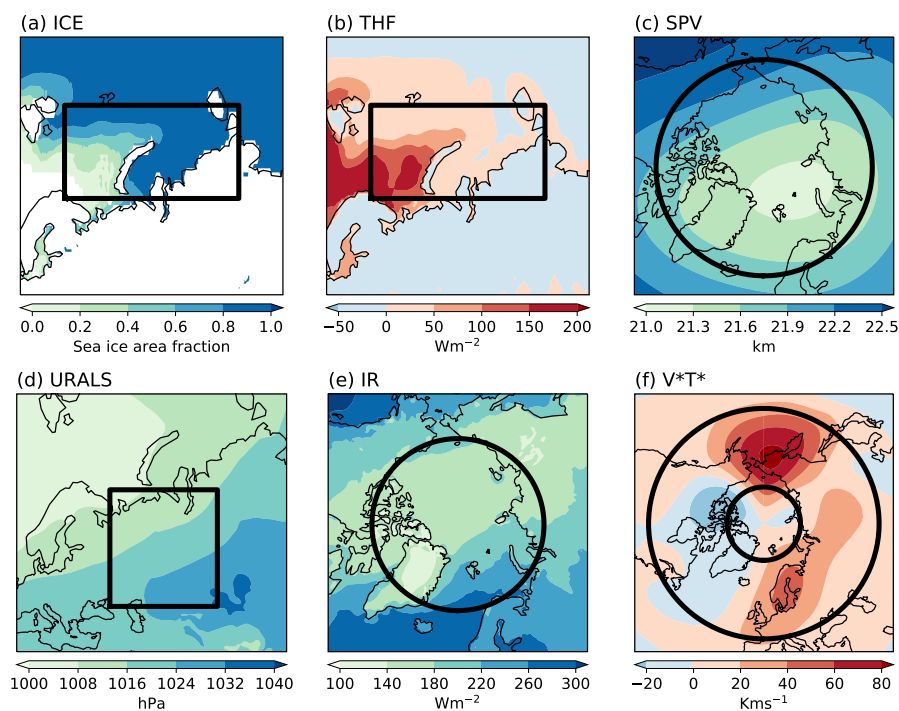
**Figure 2.** ERA-Interim (1979-2018) DJF climatologies (shading) of key variables and regions (black boxes) for computing area-averaged indices: (a) Sea ice area fraction, 70°-80° N, 30°-105° E, (b) Turbulent heat flux, 70°-80° N, 30°-105° E, (c) Stratospheric polar vortex, which is defined by 10-100 hPa geopotential height, 65°-90° N, (d) Urals sea level pressure, 45°-70° N, 40°-85° E, (e) Downward longwave radiation, 70°-90° N, (f) 100 hPa poleward eddy heat flux, 45°-75° N. For (b), turbulent heat flux from the ocean to the atmosphere is defined as positive. See section 2.1 for details.
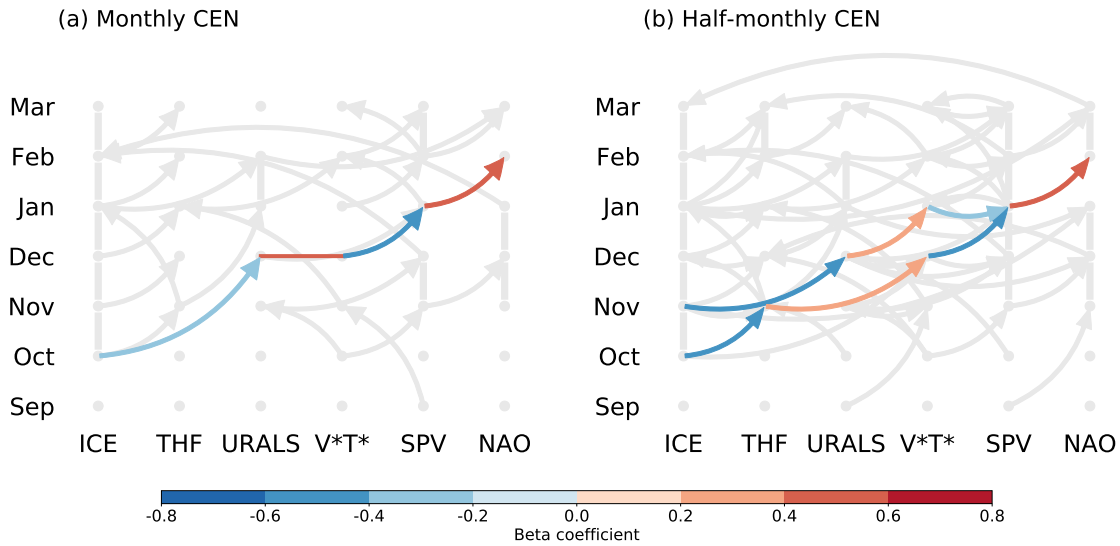
**Figure 3.** Seasonal evolution of the stratospheric pathway (indicated by coloured arrows) detected by the (a) monthly and (b) half-monthly CENs. Arrows indicate causal linkages; vertical lines indicate auto-correlation; horizontal bars indicate simultaneous relationships; colours show the sign and strength of the linkages as given by the CEN beta coefficients (see section 2.2). The grey background shows other significant linkages (arrows) and autocorrelations (vertical lines), but does not include simultaneous relationships. The half-monthly CEN in (b) has been aggregated into full months for ease of comparison with (a); see Fig. S2 for unaggregated version.
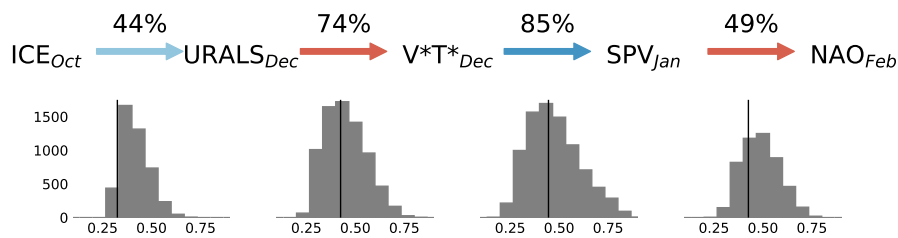
**Figure 4.** Results of a bootstrapping test to assess the robustness of causal linkages within the stratospheric pathway. Percentages above arrows show the occurrence rate of each linkage out of 10,000 bootstrap samples. Colours of the arrows indicate beta coefficients values as in Figure 3a. Histograms below show the corresponding distribution of beta coefficients (absolute value) in the bootstrap samples. Note that the distributions are composed only of samples that detect the linkages.
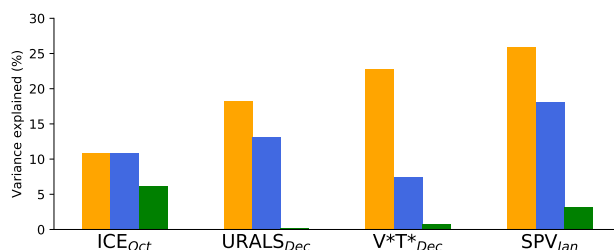
**Figure 5.** Explanatory power of the stratospheric pathway for the February NAO assessed via multiple linear regression. Orange bars show the cumulative variance explained when including each regressor in succession from left to right; blue bars show variance explained by the individual regressor; green bars show the reduction in total variance explained when removing that regressor. See section 3.3 for details.
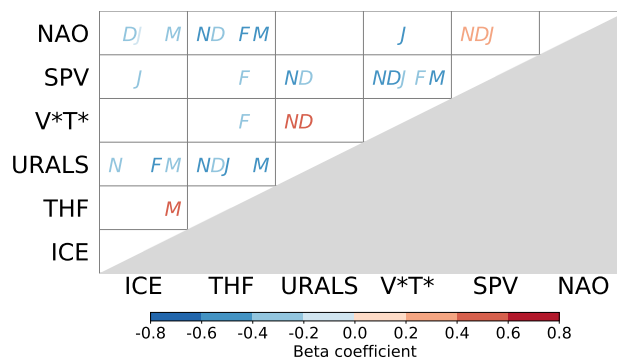
**Figure 6.** Simultaneous relationships between monthly indices in November (N), December (D), January (J), February (F) and March (M). Colours indicate the sign and strength of the relationship as given by the CEN beta coefficients (see section 2.2)

.
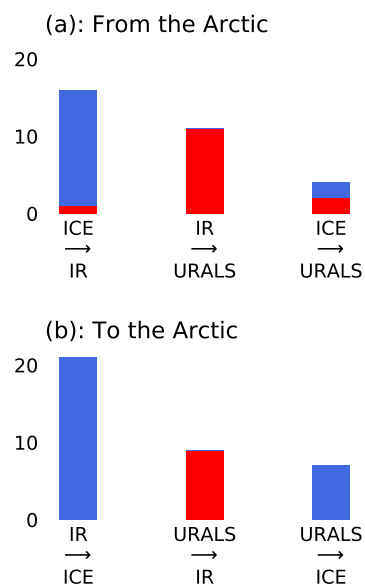
**Figure 7.** Results of the pentad CEN analysis assessing relationships between downward longwave radiation (IR), Barents-Kara sea ice (ICE) and Urals sea level pressure (URALS). (a) Linkages from the Arctic to the midlatitudes. (b) Linkages from the midlatitudes to the Arctic. Red (blue) colours denote positive (negative) relationships. The pentad results shown here have been aggreated over the October-to-March cold season; see Fig. S6 for unaggregated version.